

Heterogeneous & Homogeneous & Bio- & Nano-

CHEM **CAT** CHEM

CATALYSIS

Accepted Article

Title: Transient in-situ DRIFTS investigation of catalytic oxidation of toluene over α -, γ - and β -MnO₂

Authors: Jie Fan, Quanming Ren, Shengpeng Mo, Yuhang Sun, Mingli Fu, Junliang Wu, Limin Chen, Peirong Chen, and Daiqi Ye

This manuscript has been accepted after peer review and appears as an Accepted Article online prior to editing, proofing, and formal publication of the final Version of Record (VoR). This work is currently citable by using the Digital Object Identifier (DOI) given below. The VoR will be published online in Early View as soon as possible and may be different to this Accepted Article as a result of editing. Readers should obtain the VoR from the journal website shown below when it is published to ensure accuracy of information. The authors are responsible for the content of this Accepted Article.

To be cited as: *ChemCatChem* 10.1002/cctc.201901839

Link to VoR: <http://dx.doi.org/10.1002/cctc.201901839>

FULL PAPER

Transient in-situ DRIFTS investigation of catalytic oxidation of toluene over α -, γ - and β -MnO₂

Jie Fan,^[a] Quanming Ren,^[a] Shengpeng Mo,^[a] Yuhang Sun,^[a] Mingli Fu,^[a,b,c] Junliang Wu,^[a,b,c] Limin Chen,^[a,b,c] Peirong Chen,^[a,b,c] and Daiqi Ye*^[a,b,c]

Abstract: Manganese oxides with different crystal phases (i.e. α -MnO₂, γ -MnO₂ and β -MnO₂) were synthesized for catalytic oxidation of toluene. The catalytic activity was strongly influenced by the crystal phases of MnO₂. α -MnO₂ exhibited the highest catalytic activity with a 50% toluene conversion (T₅₀) at 229 °C and a 90% toluene conversion (T₉₀) at 238 °C, followed by γ -MnO₂ (T₉₀=252 °C) and β -MnO₂ (T₉₀=278 °C). The remarkable catalytic activity of α -MnO₂ was attributed to its superior redox property and lattice oxygen mobility. Different intermediates were detected on the surfaces of α -, γ - and β -MnO₂ by in situ diffuse reflectance infrared Fourier transform spectroscopy (in-situ DRIFTS). Benzoate species were found to be the key intermediates on α -MnO₂ at 240 °C, while benzoyl oxide species and benzoate were the major intermediates on γ -MnO₂ at 260 °C. The surface of β -MnO₂ was mainly covered by carbonate and benzoate species after the adsorption of toluene at 280 °C.

Introduction

Volatile organic compounds (VOCs), such as toluene, emitted mainly from house-hold activities and industrial processes, not only induce various atmospheric pollution problems (ozone and photochemical smog), but also severely threaten the health of human beings^[1]. Currently, numerous technologies have been investigated for VOCs control, such as adsorption, photocatalysis, photothermal catalysis and thermal catalytic oxidation^[2]. Among them, thermal catalytic oxidation of toluene into CO₂ and H₂O has been regarded as one of the most promising techniques due to its high destructive efficiency and less harmful by-products^[3]. The key issue of this technique is the development of high-performance catalysts. Although noble metal catalysts (Pt, Pd and Au, etc.) usually exhibit high removal efficiency at low

temperatures^[4], disadvantages such as high cost, easy sintering and poisoning have restricted their application. Therefore, it is highly desirable to develop economical and efficient low-temperature catalysts.

In recent decades, non-noble metal catalysts including Ce, Co, Fe and Mn-based catalysts have been studied to substitute noble metal catalysts in toluene degradation^[5]. Among them, MnO_x catalysts have been intensively investigated thanks to their remarkable low-temperature redox property, which is essential for the complete oxidation of toluene at low temperatures^[6]. Furthermore, MnO₂ with various crystallographic forms, such as α -, β -, γ -, δ - and ϵ -MnO₂, could be synthesized through the orderly arranging of [MnO₆] basic units, and they usually exhibited distinguished structures sensitive to different catalytic VOCs oxidation reactions. Hu et al.^[7] investigated the effect of crystal phase of MnO₂ on the catalytic performance of benzene combustion. The catalytic activities in benzene combustion over various manganese oxides decreased in the order: γ -MnO₂ > β -MnO₂ > α -MnO₂ > δ -MnO₂. Zeng and Xing et al.^[8] found that the higher catalytic activity in o-xylene was observed over ordered mesoporous γ -MnO₂ catalyst compared with mesoporous β -MnO₂ and nonporous α -MnO₂ nanorods. Zhang et al.^[9] explored the catalytic activity of α -, β -, γ - and δ -type MnO₂ in HCHO oxidation. The δ -MnO₂ catalyst exhibited the highest activity among the four catalysts and achieved nearly a complete HCHO conversion at 80 °C. It was believed that the tunnel structure and active lattice oxygen species were the main factors that determined the excellent performance of δ -MnO₂. Li et al.^[10] verified the important promoting effect of oxygen vacancies for the remarkable low-temperature catalytic activity in toluene oxidation through a comparative study of δ - and β -MnO₂. δ -MnO₂ with abundant oxygen vacancies presented a higher catalytic activity. Yet, effect of crystal phase of MnO₂ was mainly investigated in catalytic oxidation of benzene, o-xylene, HCHO and toluene, and mainly focused on the structure-performance relationship. Less attention has been paid to the reactivity of adsorbed surface species on manganese oxides with different crystal phases during the catalytic oxidation reactions. Considering that the understanding of the reaction mechanism is crucial for the targeted design of high-performance catalysts for toluene oxidation, it is necessary to explore the reactivity of adsorbed surface species during toluene oxidation over manganese oxides with different crystal phases.

In the present work, a series of manganese oxides with different crystal phases, including α -MnO₂, γ -MnO₂ and β -MnO₂, were successfully synthesized and applied in the catalytic oxidation of toluene. The synthesized manganese oxides were investigated by X-ray diffraction, Scanning electron microscopy, Transmission electron microscopy, H₂ temperature-programmed

[a] J. Fan, Q. Ren, S. Mo, Y. Sun, M. Fu, J. Wu, L. Chen, P. Chen and Prof. D. Ye
School of Environment and Energy
South China University of Technology
Guangzhou, 510006, China
E-mail: cedqye@scut.edu.cn

[b] M. Fu, J. Wu, L. Chen, P. Chen and Prof. D. Ye
Guangdong Provincial Key Laboratory of Atmospheric Environment and Pollution Control (SCUT)
South China University of Technology
Guangzhou, 510006, China

[c] M. Fu, J. Wu, L. Chen, P. Chen and Prof. D. Ye
National Engineering Laboratory for VOCs Pollution Control Technology and Equipment
South China University of Technology
Guangzhou, 510006, China

Supporting information for this article is given via a link at the end of the document.

FULL PAPER

reduction, O₂ temperature-programmed desorption and X-ray photoelectron spectroscopy. The reactivity of different adsorbed surface species over α -MnO₂, γ -MnO₂ and β -MnO₂ were studied by in situ diffuse reflectance infrared Fourier transform spectroscopy (in-situ DRIFTS).

Results and Discussion

3.1 Catalytic performance

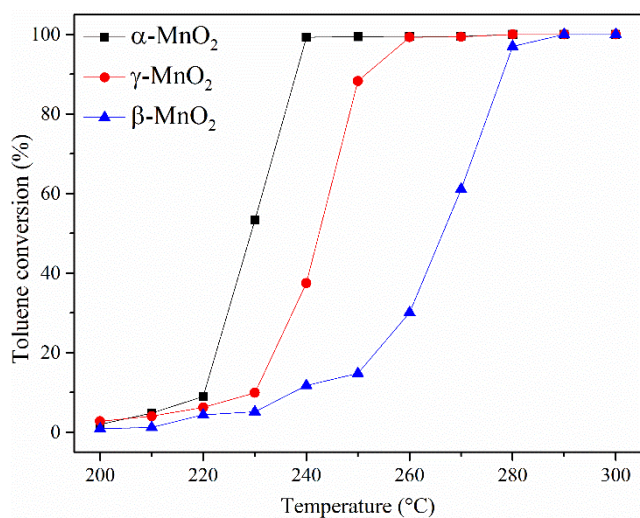


Figure 1. Conversion of toluene oxidation over α -MnO₂, γ -MnO₂ and β -MnO₂. Reaction conditions: 0.1 g catalyst and 0.4 g quartz sands, 1000 ppm toluene, 20% O₂/N₂ and WHSV = 48,000 mL·g⁻¹·h⁻¹.

The catalytic activity of manganese oxides (α , β and γ -MnO₂) with different crystal phases was evaluated in toluene oxidation and the results are shown in Figure 1. It could be found that toluene could be completely decomposed into CO₂ and H₂O over all the samples below 290 °C. Notably, among these catalysts, α -MnO₂ exhibited the highest toluene conversion at the lowest temperature with T₅₀ = 229 °C and T₉₀ = 238 °C. The catalytic activity of other samples was followed by γ -MnO₂ (T₅₀=243 °C and T₉₀=252 °C) and β -MnO₂ (T₅₀=266 °C and T₉₀=278 °C). The T₉₀ of α -MnO₂ was 40 °C lower than that of β -MnO₂, indicating the activity of above manganese oxides was strongly influenced by their crystal phases. Particularly, the fastest light-off rate over α -MnO₂ could be achieved within 20 °C from toluene conversion of 9% to 100%, which further confirmed the significant influence of crystal phases of MnO₂ in toluene oxidation. The CO₂ yield was calculated to evaluate the CO₂ selectivity of toluene oxidation over α -, γ - and β -MnO₂ catalysts. As presented in Figure S1, nearly 100% CO₂ yield was achieved over the three samples at temperatures with complete toluene conversion, indicating all the catalysts exhibited an excellent CO₂ selectivity.

3.2 Structural and morphological analysis

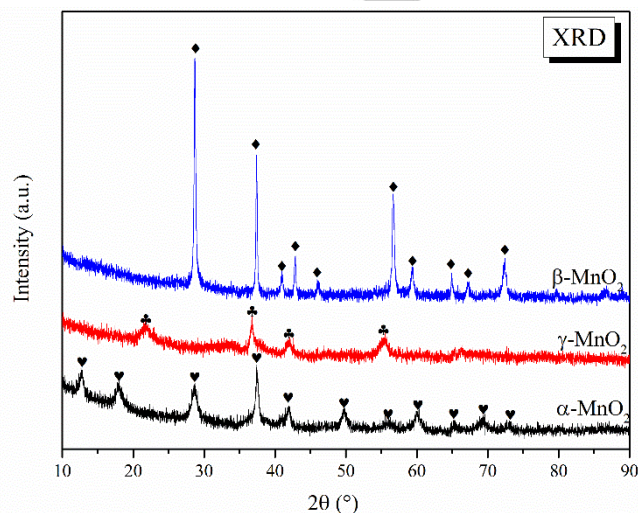


Figure 2. XRD patterns of α -MnO₂, γ -MnO₂ and β -MnO₂

The XRD of α -MnO₂, γ -MnO₂ and β -MnO₂ are depicted in Figure 2. Compared with the standard XRD patterns, α -MnO₂ and β -MnO₂ showed well-defined diffraction characteristics of tetragonal cryptomelane type α -MnO₂ (JCPDS NO 44-0141) and pyrolusite β -MnO₂ (JCPDS NO 24-0735), respectively [11]. However, compared with that of α -MnO₂ and β -MnO₂, diffraction peaks for γ -MnO₂ (JCPDS NO 14-0644) were greatly lower in intensity and broader in width, implying the poor crystallinity of γ -MnO₂. The results of XRD demonstrated the successful synthesis of α -MnO₂, γ -MnO₂ and β -MnO₂.

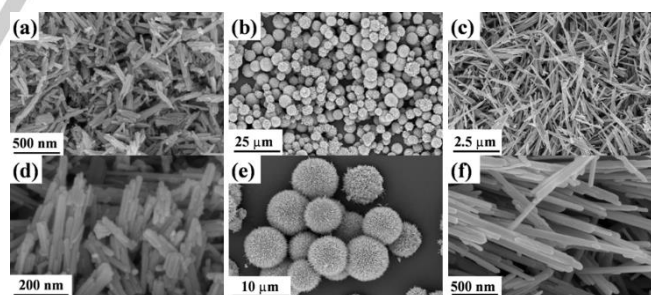


Figure 3. SEM images of (a, d) α -MnO₂, (b, e) γ -MnO₂ and (c, f) β -MnO₂.

The morphologies of above manganese oxides with different crystal phases were characterized by SEM, as presented in Figure 3. It could be clearly seen from Figure 3 a-c and the partial enlarged images (Figure 3 d-f), that nanometer multi-rod linkages, urchins self-assembled by nanorods, straight nanorods were achieved over α -MnO₂, γ -MnO₂ and β -MnO₂ samples, respectively. TEM and HRTEM were performed to further identify the structure and exposed facets of these manganese oxides. As

FULL PAPER

shown in Figure 4 a-c, similar morphologies as the SEM images were observed in TEM images. From the HRTEM images (Figure 4 d-f), well-resolved lattice fringes could be identified. The lattice spacings of 0.308, 0.490 and 0.695 nm could be indexed to the (310), (200) and (110) planes, respectively, of standard α -MnO₂ (JCPDS NO 44-0141). The lattice spacing of 0.243 nm was assigned to the (131) plane of γ -MnO₂ (JCPDS NO 14-0644), while the lattice spacing of 0.312 nm was ascribed to the (110) plane of β -MnO₂ (JCPDS NO 24-0735).

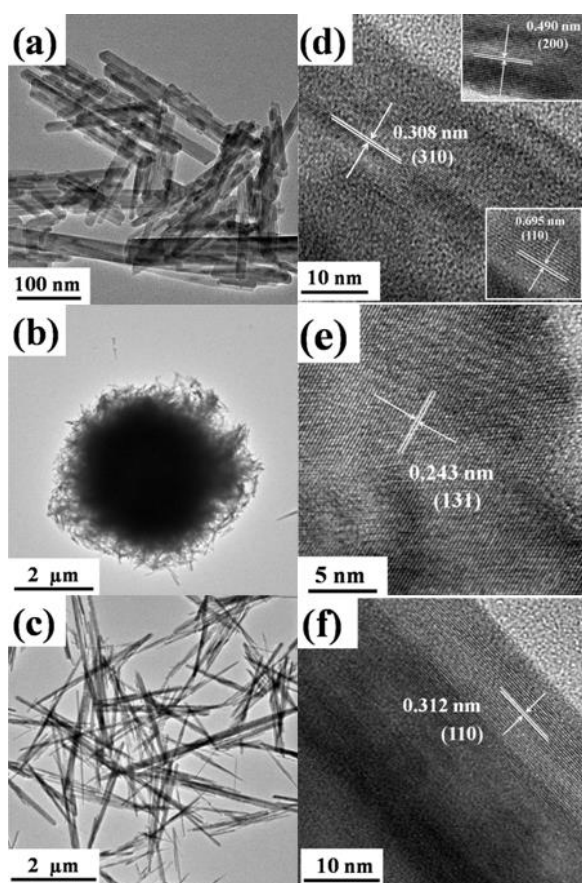


Figure 4. TEM and HRTEM of (a, d) α -MnO₂, (b, e) γ -MnO₂ and (c, f) β -MnO₂.

To further understand the subtle phase information of as-synthesized catalysts, Raman spectroscopy analysis was conducted over α -MnO₂, γ -MnO₂ and β -MnO₂. As displayed in Figure S2, the most intensive Raman band at 652 cm⁻¹ was detected over all the samples, and two small Raman bands at 576 and 580 cm⁻¹ were observed on the α -MnO₂ and γ -MnO₂ samples, respectively. The Raman band at 652 cm⁻¹ could be assigned to the symmetric stretching vibrations ($\nu_2(\text{Mn-O})$) perpendicular to the direction of the MnO₆ octahedral double chains, indicating the formation of III or IV manganese oxides [12]. The Raman peak at 580 cm⁻¹ was the characteristic feature of MnO₂ for cryptomelane type α -MnO₂ and the Raman peak at 576 cm⁻¹ belonged to the ramsdellite γ -MnO₂ [11b, 13], which was in agreement with the results of XRD.

The N₂ adsorption-desorption isotherms of as-synthesized catalysts are illustrated in Figure S3. According to the IUPAC classification, all of the samples exhibited type-IV adsorption isotherms with an obvious type H₃ hysteresis loops, indicating the presence of irregular pore structure [14]. The different size of hysteresis loops over various manganese oxides contributed to the distinguishing textural properties. As summarized in Table 1, the α -MnO₂ possessed the largest specific surface area (83 m²·g⁻¹) and pore volume (0.53 m³·g⁻¹), which might facilitate the mass transfer and provide adequate sites for toluene adsorption. Besides, the specific surface area and pore volume of other samples decreased in the order of γ -MnO₂ (63 m²·g⁻¹ and 0.25 m³·g⁻¹) > β -MnO₂ (12 m²·g⁻¹ and 0.12 m³·g⁻¹). This is in line with the sequence of decreasing activity. In order to exclude the effect of BET, the specific reaction rate (r_{norm} , conversion normalized by specific surface area) was calculated and the result was plotted in Figure S4. It can be seen that a higher r_{norm} was obtained over α -MnO₂, indicating that the specific surface area was not the key factor affecting catalytic activity.

3.3 H₂-TPR and O₂-TPD

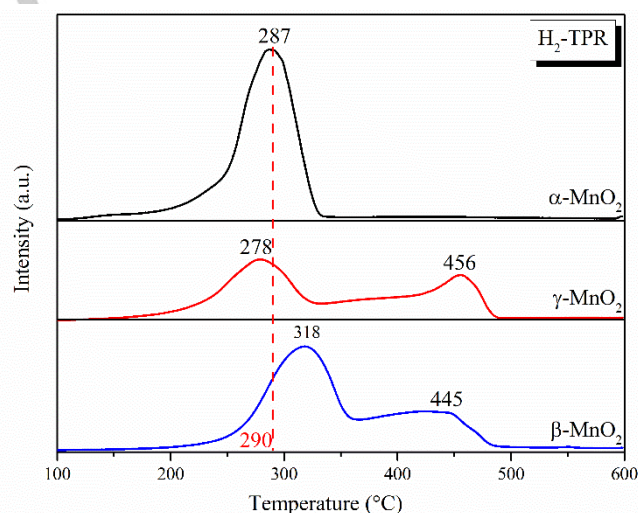


Figure 5. H₂-TPR profiles of α -MnO₂, γ -MnO₂ and β -MnO₂.

H₂-TPR was employed to investigate the redox properties of as-synthesized catalysts. As illustrated in Figure 5, two separated H₂ consumption peaks were detected over γ -MnO₂ (278 and 456 °C) and β -MnO₂ (318 and 445 °C), belonging to the stepwise reduction of Mn⁴⁺ to Mn³⁺ and Mn³⁺ to Mn²⁺, respectively [9, 15]. Different from other samples, only one strong H₂ consumption peak centered at 287 °C was observed over α -MnO₂, indicating that Mn⁴⁺ was completely reduced to Mn²⁺ below 350 °C [16]. The mobility of oxygen plays an important role in the catalytic oxidation of VOCs [17]. The easier complete reduction of Mn⁴⁺ at lower temperatures reflected the excellent mobility of lattice oxygen over α -MnO₂ sample, resulting in the most outstanding activity for

FULL PAPER

toluene oxidation (Figure 1). In addition, the descending order of H_2 consumption below 290 °C (the temperature required for complete conversion of toluene for all catalysts) was in good agreement with the descending order of catalytic activity (as shown in Figure 1), implying the superior redox ability of α - MnO_2 made for the highest catalytic activity. To further understand the effect of redox property on the catalytic performance, the low-temperature reducibility of these samples was compared by the value of onset reduction temperature. It was worth noting that the sequence of onset reduction temperature was followed as α - MnO_2 (129 °C) < γ - MnO_2 (172 °C) < β - MnO_2 (209 °C). This order was consistent with the sequence of the catalytic activity of different manganese oxides in Figure 1. Consequently, the redox properties of manganese oxides with different crystal phases were significantly different, the higher the low-temperature reducibility, the higher the catalytic activity at low temperatures.

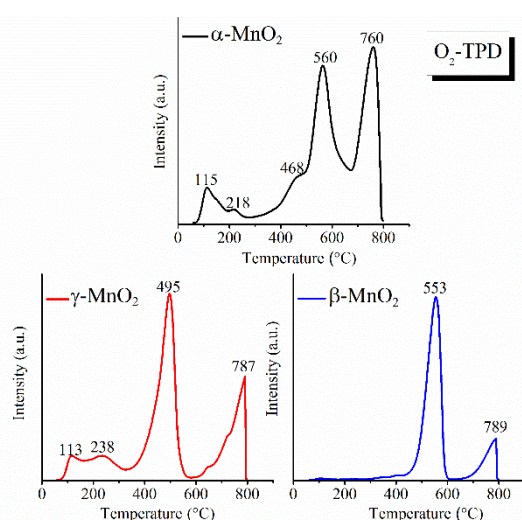


Figure 6. O_2 -TPD profiles of α - MnO_2 , γ - MnO_2 and β - MnO_2 .

Figure 6 displays the O_2 -TPD profiles of manganese oxides with different crystal phases. The type and amount of oxygen species on the catalysts could be distinguished according to the O_2 desorption peaks in different temperature regions. Based on the previous studies, the O_2 desorption peak below 300 °C could be attributed to the physisorbed molecular oxygen (<200 °C) or active surface oxygen species, while the peaks at above 600 °C resulted from the release of bulk lattice oxygen^[18]. The desorption peaks located in the medium temperature region (300-600 °C) could be assigned to the subsurface lattice oxygen, which was known to be relatively active and could notably affect the catalytic activity^[19]. By contrast, the bulk lattice oxygen received less attention due to its weaker reactivity. As shown in Figure 6, both the physisorbed molecular oxygen and active surface oxygen species were detected over α - MnO_2 and γ - MnO_2 (but not over β - MnO_2) in the low-temperature regions at 113-115 °C and 218-238 °C, respectively. The absence of active surface oxygen species at low temperatures over β - MnO_2 might be responsible for its inferior catalytic activity compared with the other samples

(Figure 1), since active surface oxygen played an important role in the catalytic oxidation reaction^[20]. As for medium temperature regions, the subsurface lattice oxygen desorption peaks centered at 560 °C (with a shoulder peak at 468 °C), 495 °C and 553 °C for α - MnO_2 , γ - MnO_2 and β - MnO_2 , respectively. Obviously, the maximum desorption peak area was found to result from subsurface lattice oxygen on the three catalysts, indicating a high availability of the subsurface lattice oxygen. Noticeably, there were considerable amount of subsurface lattice oxygen desorbed from α - MnO_2 at 468 °C. Compared with other samples, the relatively low oxygen desorption temperature at 468 °C on α - MnO_2 reflected a better mobility of subsurface lattice oxygen. This superiority could be responsible (at least partially) for the high catalytic activity of α - MnO_2 in toluene oxidation.

3.4 XPS results

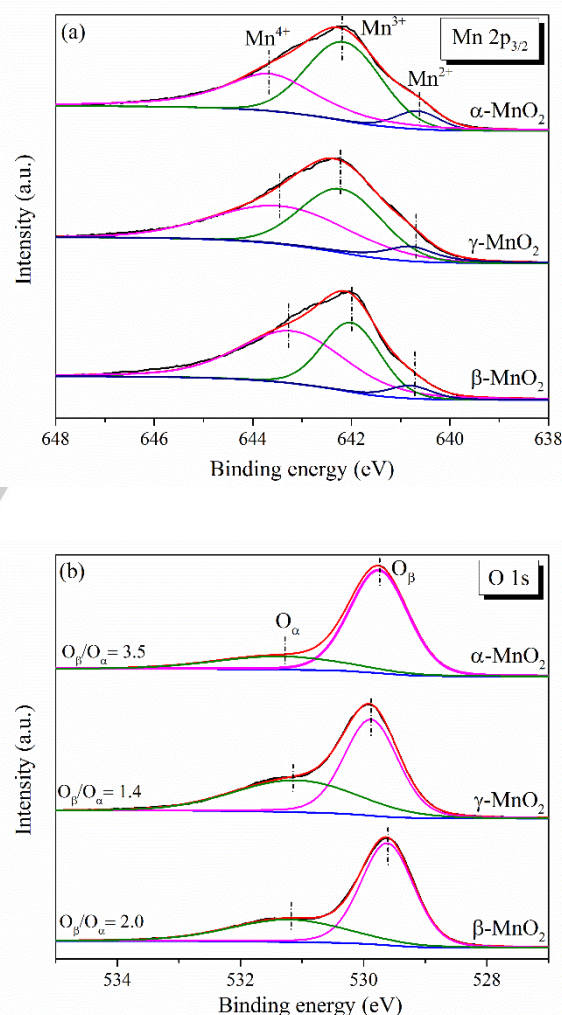


Figure 7. (a) Mn $2p_{3/2}$ and (b) O $1s$ XPS of α - MnO_2 , γ - MnO_2 and β - MnO_2 .

FULL PAPER

XPS was used to probe the surface chemical states and atomic concentrations of different manganese oxides, and the results are presented in Figure 7 and Table 1. As shown in Figure 7 (a), the Mn 2p_{3/2} XPS spectra of all the samples were split into three banding energy peaks. The binding energy peaks at 640.7-640.8, 642.1-642.2 and 643.4-643.6 eV could be ascribed to the surface Mn²⁺, Mn³⁺ and Mn⁴⁺ species, respectively, revealing the co-existence of three kinds of Mn species on the surface of α-MnO₂, γ-MnO₂ and β-MnO₂ [21]. The relative surface contents of (Mn²⁺+Mn³⁺)/Mn_{total} based on the XPS peak areas were summarized in Table 1. It was found that the ratios of (Mn²⁺+Mn³⁺)/Mn_{total} varied with the change of crystal phase of manganese oxides. The highest (Mn²⁺+Mn³⁺)/Mn_{total} ratio of 0.58 was achieved on the surface of α-MnO₂, implying more surface oxygen vacancies existed in α-MnO₂ [10], which was beneficial for the catalytic oxidation of toluene.

Figure 7 (b) presents the O 1s XPS spectra of the three catalysts, which were fitted into two distinct peaks, corresponding to the surface chemisorbed oxygen O_a (531.3-531.4 eV) with low coordination and lattice oxygen O_β (529.6-529.9 eV), respectively [22]. The ratios of O_β/O_a were calculated and shown in Figure 7(b), which was followed the sequence: α-MnO₂ (3.5) > β-MnO₂ (2.0) > γ-MnO₂ (1.4). It has been intensively reported that, as for manganese oxides catalysts, the concentration of lattice oxygen could dominate the activity during the oxidation reactions, such as CO and HCHO oxidation, which followed the Mars-van Krevelen mechanism [23]. Zhang et al. [9] found that active lattice oxygen species were the main influential factor for the excellent performance of HCHO oxidation over δ-MnO₂. This phenomenon could also be partially verified by the present work, namely, α-MnO₂ with the highest O_β concentration of 3.5 (in Figure 7b) presented the highest toluene oxidation activity among the three catalysts (in Figure 1). However, similar conclusions were not valid for γ-MnO₂ and β-MnO₂. Hence the reaction process between toluene and oxygen species over manganese oxides with different crystal phases should be further investigated.

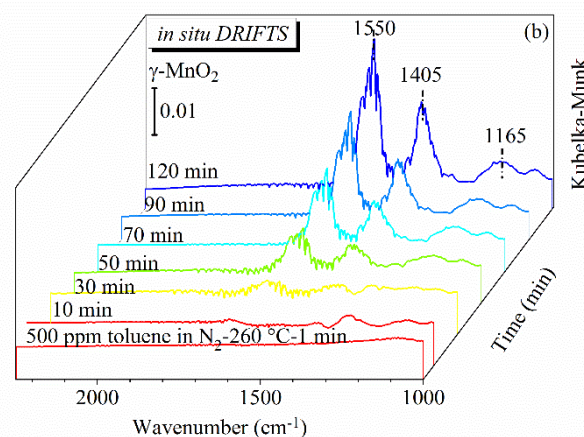
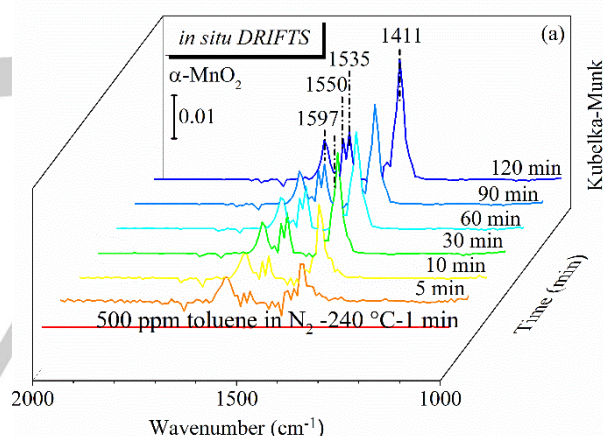
3.5 Transient in-situ DRIFTS studies

3.5.1 Adsorption of toluene

In-situ DRIFTS is a powerful tool for studying reaction mechanism, and can give insights into the transformation processes of toluene and oxygen species. Thus, the α-MnO₂, γ-MnO₂ and β-MnO₂ catalysts were further studied by in-situ DRIFTS.

In-situ DRIFTS spectra of 500 ppm toluene adsorption over α-MnO₂, γ-MnO₂ and β-MnO₂ samples were recorded to identify the adsorbed surface species. As shown in Figure 8 (a), four stable adsorption bands were detected over α-MnO₂ at 1411, 1535, 1550 and 1597 cm⁻¹ after toluene adsorption at 240 °C for 120 min. The band at 1411 cm⁻¹ could be attributed to the symmetrical vibration of COO⁻, indicating the potential existence of benzoate. The bands at 1535 and 1550 cm⁻¹ were ascribed to the asymmetric C-O stretching vibration, indicating the formation

of benzoate on the surface of α-MnO₂, while the band at 1597 cm⁻¹ was attributed to ν(C=C) of the skeletal vibrations of the aromatic rings [24]. As for γ-MnO₂ presented in Figure 8 (b), the adsorption of toluene at 260 °C gave rise to two adsorption bands different from those for α-MnO₂, the band at 1165 cm⁻¹ was assigned to C-O bond of benzoyl oxide species (C₆H₅-CH₂-O), whereas the band at 1405 cm⁻¹ was ascribed to symmetrical vibration of COO⁻ [12b, 24b, 25], implying the formation of benzoate. In the case of β-MnO₂ shown in Figure 8(c), the band at 1025 cm⁻¹ was assigned to the C-H in-plane bending vibration of benzene rings, while the bands at 1249 cm⁻¹ belonged to the carbonate species, respectively [24a, 24d, 26]. The band at 1412 cm⁻¹ could be attributed to symmetrical vibration of COO⁻, implying the formation of benzoate. Evidently, different chemisorbed modes of benzene rings contained species were detected on the surfaces of α-, γ- and β-MnO₂, respectively. The benzoate species were the main adsorbed surface species on α-MnO₂ at 240 °C, while benzoyl oxide species and benzoate were the major adsorbed surface species on γ-MnO₂ at 260 °C. The surface of β-MnO₂ was mainly covered by carbonate and benzoate species after the adsorption of toluene at 280 °C.



FULL PAPER

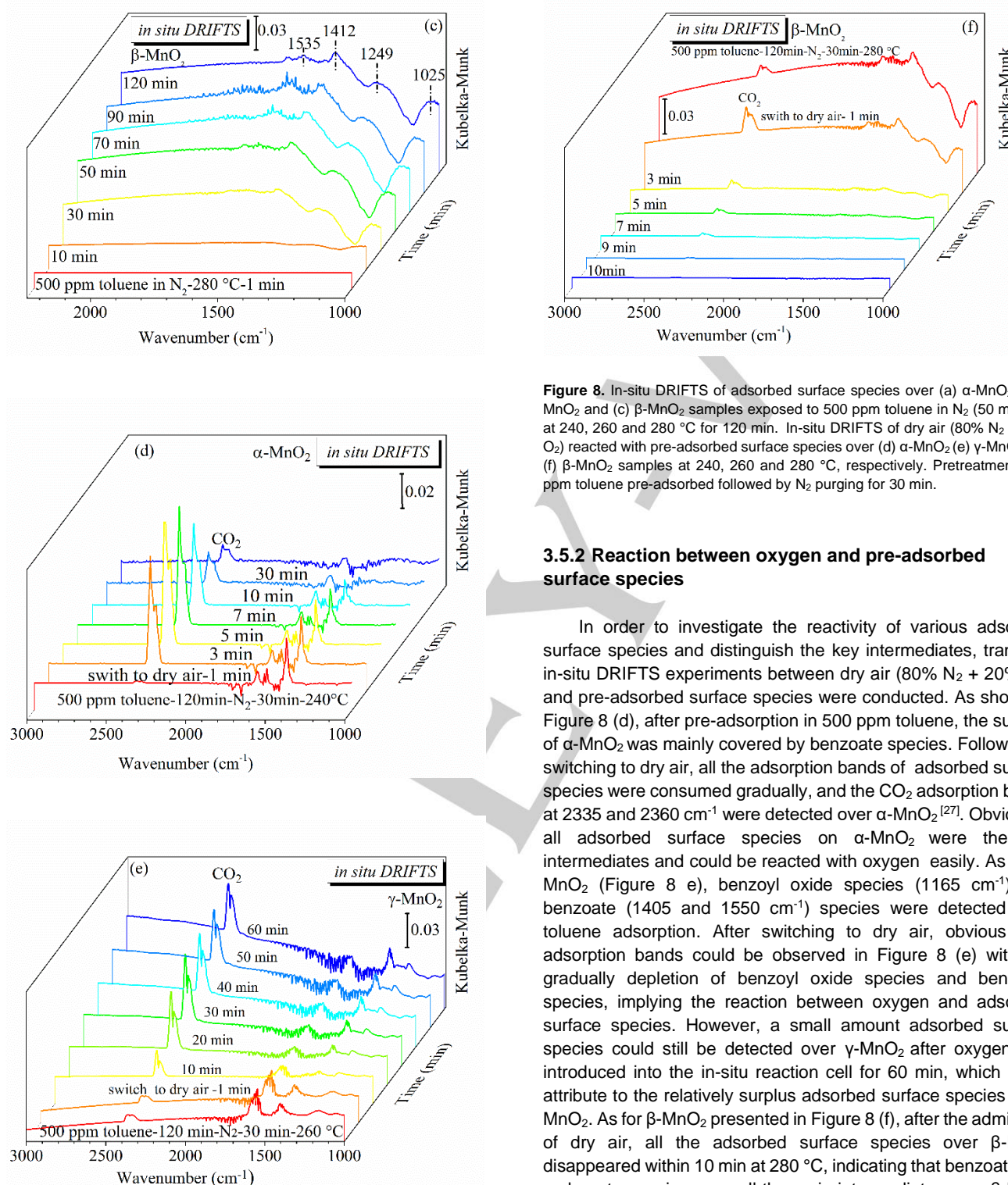


Figure 8. In-situ DRIFTS of adsorbed surface species over (a) α -MnO₂ (b) γ -MnO₂ and (c) β -MnO₂ samples exposed to 500 ppm toluene in N₂ (50 mL/min) at 240, 260 and 280 °C for 120 min. In-situ DRIFTS of dry air (80% N₂ + 20% O₂) reacted with pre-adsorbed surface species over (d) α -MnO₂ (e) γ -MnO₂ and (f) β -MnO₂ samples at 240, 260 and 280 °C, respectively. Pretreatment: 500 ppm toluene pre-adsorbed followed by N₂ purging for 30 min.

3.5.2 Reaction between oxygen and pre-adsorbed surface species

In order to investigate the reactivity of various adsorbed surface species and distinguish the key intermediates, transient in-situ DRIFTS experiments between dry air (80% N₂ + 20% O₂) and pre-adsorbed surface species were conducted. As shown in Figure 8 (d), after pre-adsorption in 500 ppm toluene, the surface of α -MnO₂ was mainly covered by benzoate species. Followed by switching to dry air, all the adsorption bands of adsorbed surface species were consumed gradually, and the CO₂ adsorption bands at 2335 and 2360 cm⁻¹ were detected over α -MnO₂^[27]. Obviously, all adsorbed surface species on α -MnO₂ were the key intermediates and could be reacted with oxygen easily. As for γ -MnO₂ (Figure 8 e), benzoyl oxide species (1165 cm⁻¹) and benzoate (1405 and 1550 cm⁻¹) species were detected after toluene adsorption. After switching to dry air, obvious CO₂ adsorption bands could be observed in Figure 8 (e) with the gradually depletion of benzoyl oxide species and benzoate species, implying the reaction between oxygen and adsorbed surface species. However, a small amount adsorbed surface species could still be detected over γ -MnO₂ after oxygen was introduced into the in-situ reaction cell for 60 min, which might attribute to the relatively surplus adsorbed surface species on γ -MnO₂. As for β -MnO₂ presented in Figure 8 (f), after the admission of dry air, all the adsorbed surface species over β -MnO₂ disappeared within 10 min at 280 °C, indicating that benzoate and carbonate species were all the main intermediates over β -MnO₂ at 280 °C.

FULL PAPER

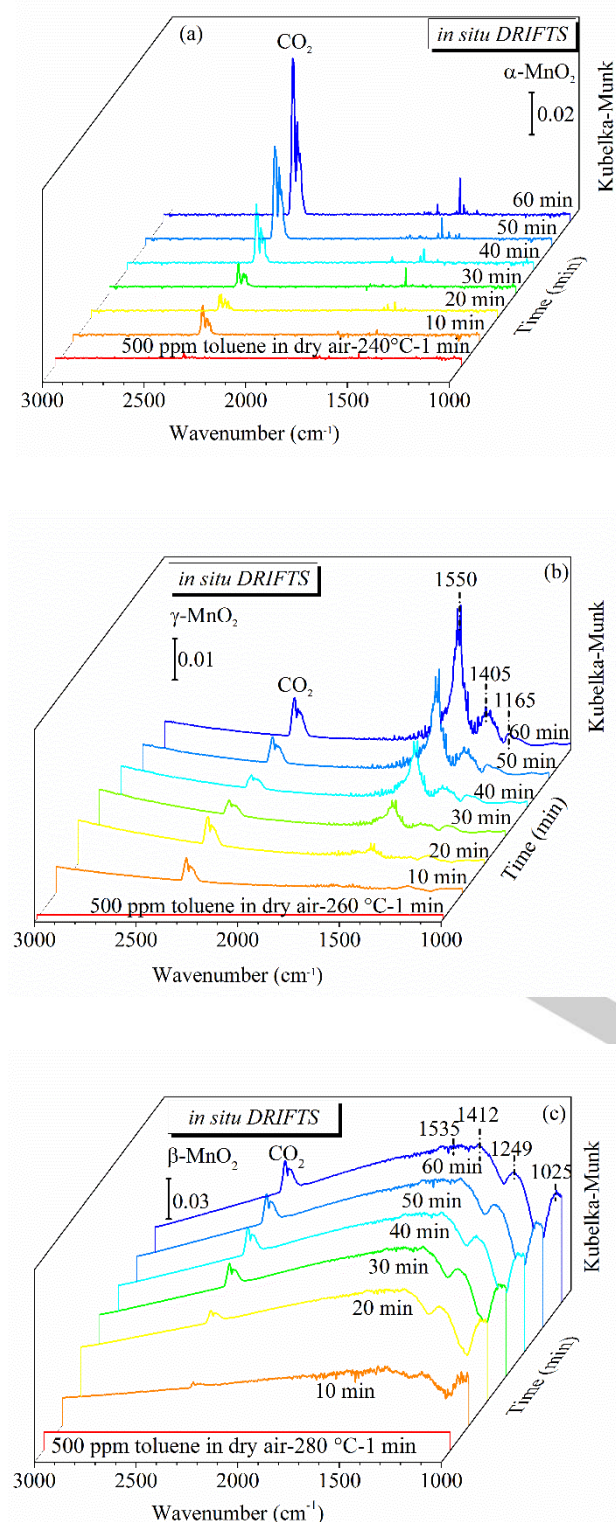


Figure 9. in-situ DRIFTS of adsorbed surface species over (a) α -MnO₂ (b) γ -MnO₂ and (c) β -MnO₂ samples arising from adsorption and reaction of 500 ppm toluene in dry air (80% N₂ + 20% O₂) at 240, 260, 280 °C, respectively.

3.5.3 Adsorption and reaction of toluene in dry air (80% N₂ + 20% O₂)

Figure 9 presents the in-situ DRIFTS of adsorbed surface species arising from α -MnO₂, γ -MnO₂ and β -MnO₂ treated with 500 ppm toluene in dry air (80% N₂ + 20% O₂) at 240, 260 and 280 °C, respectively. It could be seen from Figure 9 (a), only CO₂ was detected on α -MnO₂ throughout the whole test and the intensity of CO₂ increased with time, demonstrating that intermediates on the surface of α -MnO₂ exhibited high reactivity and could be quickly reacted with oxygen species. This phenomenon could be attributed to the superior reducibility and high mobility of lattice oxygen of α -MnO₂, which resulted in the more easier oxidation of intermediates by oxygen species on the surface of α -MnO₂. As for γ -MnO₂, besides CO₂, adsorption bands as in Figure 8 (b) were also detected on γ -MnO₂ (Figure 9b) during the co-adsorption of toluene and O₂. This observation not only further confirmed that benzoyl oxide species and benzoate species were easily adsorbed and accumulated on γ -MnO₂, but also illustrated that benzoyl oxide species and benzoate species were the major intermediates in toluene oxidation over γ -MnO₂. Similar to γ -MnO₂, the same adsorbed surface species shown in Figure 8 (c) were observed over β -MnO₂ (Figure 9c) and the intensity of CO₂ also increased with the time. Based on the above discussion of Figure 8 and 9, it could be concluded that all the adsorbed surface species on α -MnO₂, γ -MnO₂ and β -MnO₂ were the active intermediates in toluene oxidation. Injecting toluene and oxygen into the in-situ reaction cell simultaneously led to the fastest consumption of intermediates on α -MnO₂ catalyst.

Table 1. Specific surface area, Pore volume, H₂ consumption and (Mn²⁺+Mn³⁺)/Mn_{total} of all the samples.

Catalyst	Specific surface area (m ² ·g ⁻¹)	Pore volume (m ³ ·g ⁻¹)	H ₂ ^[a] consumption (mmol·g ⁻¹)	(Mn ²⁺ +Mn ³⁺)/Mn _{total}
α -MnO ₂	83	0.53	8.06	0.58
γ -MnO ₂	63	0.25	4.07	0.53
β -MnO ₂	12	0.12	2.42	0.42

[a] H₂ consumption below 290 °C.

Conclusions

A series of manganese oxides with different crystal phases (α -, γ - and β -MnO₂) were successfully synthesized and were employed in the deep oxidation of toluene. α -MnO₂ exhibited the highest catalytic activity with a T₅₀ at 229 °C and a T₉₀ at 238 °C. The T₉₀ of different manganese oxides was followed the sequence: α -MnO₂ < γ -MnO₂ < β -MnO₂. The outstanding catalytic activity of α -MnO₂ could be attributed to the excellent redox properties and the high mobility of lattice oxygen. Transient in-situ DRIFTS studies illustrated that all the adsorbed surface species

FULL PAPER

were active intermediates for toluene oxidation on α -MnO₂, γ -MnO₂ and β -MnO₂. Monitoring the reaction between pre-adsorbed surface species and oxygen by in-situ DRIFTS verified that benzoate species were the key intermediates on α -MnO₂, while benzoyl oxide species and benzoate species were the major intermediates of toluene oxidation over γ -MnO₂. For β -MnO₂, carbonate and benzoate species were the main intermediates.

Experimental Section

Catalyst preparation

All chemicals used were analytical reagents purchased from Shanghai Aladdin Co.Ltd. without further purification. The α -MnO₂, γ -MnO₂ and β -MnO₂ samples were synthesized via hydrothermal method. For α -MnO₂: 2.2 g KMnO₄ and 2.4 g Mn(CH₃COO)₂·4H₂O were dissolved in 32 mL deionized water under vigorous stirring. 0.5 mL HNO₃ was added into the above mixed solution and then reacted at 100 °C for 24 h in a Teflon-lined stainless steel autoclave. The α -MnO₂ was obtained by finally calcined the sample at 400 °C for 4 h. For γ -MnO₂: 1.35 g MnSO₄·H₂O and 1.83 g (NH₄)₂S₂O₈ were dissolved in 32 mL deionized water, followed by hydrothermal treatment at 90 °C for 24 h. The black powder was centrifugal washing with deionized water several times and dried at 80 °C overnight. For β -MnO₂: 8.11 g MnSO₄·H₂O, 3.19 K₂S₂O₈ and 2 mL HCl (37%) were dissolved in 60 mL deionized water. Except the hydrothermal temperature was 140 °C, the other processes were the same as the preparation of γ -MnO₂.

Catalyst characterization

The crystalline structure of different samples was identified by the X-ray diffraction (D8 advance diffractometer) with Cu K α radiation ($\lambda = 1.5418$ Å) at 40 kV and 40 mA. The 2θ was scanned from 10° to 90° with a scan interval of 0.02°. The N₂ adsorption-desorption isotherms were obtained at -196 °C on an ASAP 2020 automated gas sorption system. The specific surface areas and total pore volumes were calculated from Brunauer-Emmett-Teller (BET) and Barrett-Joyner-Halenda (BJH) methods, respectively. Raman spectra were collected using a LabRAM HR Evolution Laser Raman Spectrometer with a CCD detector. The excitation line was at 532 nm and the spectra range was 200-1000 cm⁻¹. The Scanning electron microscopy (SEM) images were obtained using a Zeiss Ultra at an accelerating voltage of 3 kV. High resolution transmission electron microscopy (HRTEM) and TEM images were recorded on JEM-2100HR (JEOL, Japan). H₂ temperature-programmed reduction experiments (H₂-TPR) were performed on a chemisorption analyzer (Micromeritics Chemisorb 2920II). The sample (20 mg) was firstly pretreated at 300 °C for 1 h under a Ar flow (30 mL/min), followed by cooled down the sample to 60 °C in Ar. Afterwards, the sample was heated at a ramping rate of 10 °C/min from 60 to 800 °C in a flow of 5% H₂/Ar (30 mL/min). The H₂ consumption below 290 °C of all the catalysts was calculated by using CuO as a calibration reference. Oxygen temperature-programmed desorption (O₂-TPD) experiments were also carried out on the above-mentioned equipment with similar pretreated progress, while changing the sample mass to 100 mg and pretreated gas to He (30 mL/min), respectively. After the sample was cooled down to 60 °C, 5% O₂/He was switched into the U-shape quartz reactor for 1 h and then swept with He for 30 min. The catalyst was heated from 60 to 800 °C in a He flow (30 mL/min) at 10 °C/min. The X-ray photoelectron spectroscopy (XPS) measurements were executed on a Thermo ESCALAB 250 with Al K α ($h\nu = 1486.6$ eV)

as the excitation source. The charging effects of all the samples were compensated by calibrating all binding energy with C1s peak at 284.8 eV.

In situ diffuse reflection infrared Fourier transform spectrum (in-situ DRIFTS) experiments were performed on a Nicolet 6700 FTIR spectrometer. Prior to each experiment, the sample was pretreated at 300 °C in N₂ (50 mL/min) for 1 h to remove trace impurities. The background spectrum was collected in flowing N₂ and automatically subtracted from the sample spectrum at the corresponding temperature. In the transient studies, the α -MnO₂, γ -MnO₂ and β -MnO₂ samples were firstly pre-exposed to a flow of 500 ppm toluene in N₂ (50 mL/min) at 240, 260 and 280 °C for 120 min, respectively. Then the sample was purged by N₂ (50 mL/min) for 30 min and subsequently switched the gas to dry air (80% N₂ + 20% O₂, 50 mL/min) for a certain time. For the co-adsorption of 500 ppm toluene + 20% O₂, the α -MnO₂, γ -MnO₂ and β -MnO₂ samples were exposed to mixed gases (50 mL/min) of 500 ppm toluene in dry air (80% N₂ + 20% O₂) at 240, 260 and 280 °C for 1 h and then the spectra were recorded.

Catalytic performance measurements

The catalytic activity tests were carried out in a fixed-bed quartz reactor (6 mm i.d.) using 0.1 g (40-60 mesh) catalyst accompanied with 0.4 g quartz sands to minimize the hot spots effect. The 80 mL/min total flow rate (containing 1000 ppm toluene, 20% O₂ and N₂ as balance) was employed to generate a weight hourly space velocity (WHSV) of 48,000 L·g⁻¹·h⁻¹. The concentrations of toluene were analyzed by an online gas chromatograph (GC-2014C, Shimadzu) equipped with two flame ionization detectors (FID). The activity data were collected after the reaction reached the steady state at each temperature for 1 h and evaluated using the T₅₀ and T₉₀, which defined as the temperature for toluene conversions of 50% and 90%, respectively. The conversion of toluene (X), yield of CO₂, normalized reaction rate r_{norm} (mol·m⁻²·s⁻¹) were calculated according to the following equations, respectively:

$$X = \frac{C_{toluene,in} - C_{toluene,out}}{C_{toluene,in}} \times 100\%$$

$$CO_2 \text{ yield} = \frac{C_{CO_2,out}}{7 \times C_{toluene,in}} \times 100\%$$

$$r_{norm} = \frac{C_{toluene,in} \times F}{m_{cat} \times S_{BET}} \times \ln\left(\frac{1}{1-X}\right)$$

where $C_{toluene,out}$ represented the outlet concentration of toluene at steady state and $C_{toluene,in}$ was the inlet concentration of toluene, $C_{CO_2,out}$ represented the CO₂ concentration in the outlet gas, F is the toluene flow rate (mol·s⁻¹), m_{cat} is the mass of catalyst (g). S_{BET} (m²·g⁻¹) is the specific surface area.

Acknowledgements

This work was supported by the National Key Research and Development Project (No. 2017YFC0212800)

Keywords: VOCs • Toluene • Manganese oxides • DRIFTS • Catalytic oxidation

- [1] Z. Ye, J. M. Giraudon, N. Nuns, P. Simon, N. De Geyter, R. Morent, J. F. Lamonier, *Appl. Catal. B.* **2018**, 223, 154-166.

FULL PAPER

- [2] a) J. J. Li, B. Weng, S. C. Cai, J. Chen, H. P. Jia, Y. J. Xu, *J. hazard. Mater.* **2018**, *342*, 661-669; b) Y. Zhang, Z. R. Tang, X. Fu, Y. J. Xu, *Appl. Catal. B.* **2011**, *106*, 445-452; c) J. J. Li, E. Q. Yu, S. C. Cai, X. Chen, J. Chen, H. P. Jia, Y. J. Xu, *Appl. Catal. B.* **2019**, *240*, 141-152.
- [3] D. Chlala, J. F. Giraudomn, N. Nuns, M. Labaki, J. F. Lamonier. *ChemCatChem*, **2017**, *9*, 2275-2283.
- [4] a) S. Xie, J. Deng, Y. Liu, Z. Zhang, H. Yang, Y. Jiang, H. Arandiyani, H. Dai, C. T. Au, *Appl. Catal. A.* **2015**, *507*, 82-90; b) T. Gan, X. Chu, H. Qi, W. Zhang, Y. Zou, W. Yan, G. Liu, *Appl. Catal. B.* **2019**, *257*, 117943; c) R. Peng, S. Li, X. Sun, Q. Ren, L. Chen, M. Fu, J. Wu, D. Ye, *Appl. Catal. B.* **2018**, *220*, 462-470.
- [5] a) L. Zhao, Z. Zhang, Y. Li, X. Leng, T. Zhang, F. Yuan, X. Niu, Y. Zhu, *Appl. Catal. B.* **2019**, *245*, 502-512; b) Q. Yang, D. Wang, C. Wang, K. Li, Y. Peng, J. Li, *ChemCatChem*, **2018**, *10*, 4838-4843; c) J. Chen, X. Chen, W. Xu, Z. Xu, J. Chen, H. Jia, J. Chen, *Chem. Eng. J.* **2017**, *330*, 281-293; d) Y. Wang, H. Arandiyani, Y. Liu, Y. Liang, Y. Peng, S. Bartlett, H. Dai, S. Rostamnia, J. Li, *ChemCatChem*, **2018**, *10*, 3429-3434.
- [6] a) Z. Sahaib, F. Puleo, J. M. Garcia-Vargas, L. Retailleau, C. Descorme, L. F. Liotta, J. L. Valverde, S. Gil, A. Giroir-Fendler, *Appl. Catal. B.* **2017**, *209*, 689-700; b) S. C. Kim, W. G. Shim, *Appl. Catal. B.* **2010**, *98*, 180-185.
- [7] Z. Hu, R. Mi, X. Yong, S. Liu, D. Li, Y. Li, T. Zhang, *ChemistrySelect*, **2019**, *4*, 473-480.
- [8] a) X. Zeng, G. Cheng, Q. Liu, W. Yu, R. Yang, H. Wu, Y. Li, M. Sun, C. Zhang, L. Yu, *Ind. Eng. Chem. Res.* **2019**, *58*, 13926-13934; b) Y. Wu, L. Guo, Z. Ma, Y. Gao, S. Xing, *Mater. Lett.* **2014**, *125*, 158-161.
- [9] J. Zhang, Y. Li, L. Wang, C. Zhang, H. He, *Catal. Sci. Technol.* **2015**, *5*, 2305-2313.
- [10] W. Yang, Z. a. Su, Z. Xu, W. Yang, Y. Peng, J. Li, *Appl. Catal. B.* **2019**, *260*, 118150.
- [11] a) Y. Meng, W. Song, H. Huang, Z. Ren, S. Y. Chen, S. L. Suib, *J. Am. Chem. Soc.* **2014**, *136*, 11452-11464; b) Y. Dong, K. Li, P. Jiang, G. Wang, H. Miao, J. Zhang, C. Zhang, *RSC Adv.* **2014**, *4*, 39167.
- [12] a) S. Rong, P. Zhang, F. Liu, Y. Yang, *ACS Catal.* **2018**, *8*, 3435-3446; b) Y. Luo, Y. Zheng, J. Zuo, X. Feng, X. Wang, T. Zhang, K. Zhang, L. Jiang, *J. hazard. Mater.* **2018**, *349*, 119-127.
- [13] F. Buciuman, F. Patcas, R. Craciun, D. R. T. Zahn, *Phys. Chem. Chem. Phys.* **1999**, *1*, 185-190.
- [14] a) J. Fan, P. Ning, Z. Song, X. Liu, L. Wang, J. Wang, H. Wang, K. Long, Q. Zhang, *Chem. Eng. J.* **2018**, *334*, 855-863; b) Z. Feng, Q. Ren, R. Peng, S. Mo, M. Zhang, M. Fu, L. Chen, D. Ye, *Catal. Today*, **2019**, *332*, 177-182.
- [15] C. Dong, Z. Qu, Y. Qin, Q. Fu, H. Sun, X. Duan, *ACS Catal.* **2019**, *9*, 6698-6710.
- [16] F. Wang, H. Dai, J. Deng, G. Bai, K. Ji, Y. Liu, *Environ. Sci. Technol.* **2012**, *46*, 4034-4041.
- [17] N. Huang, Z. Qu, C. Dong, Y. Qin, X. Duan, *Appl. Catal. A.* **2018**, *560*, 195-205.
- [18] a) L. Yu, G. Diao, F. Ye, M. Sun, J. Zhou, Y. Li, Y. Liu, *Catal. Lett.* **2010**, *141*, 111-119; b) Y. Yang, J. Huang, S. Wang, S. Deng, B. Wang, G. Yu, *Appl. Catal. B.* **2013**, *142-143*, 568-578; c) Y. Zheng, W. Wang, D. Jiang, L. Zhang, *Chem. Eng. J.* **2016**, *284*, 21-27.
- [19] F. G. Durán, B. P. Barbero, L. E. Cadús, C. Rojas, M. A. Centeno, J. A. Odriozola, *Appl. Catal. B.* **2009**, *92*, 194-201.
- [20] H. Sun, X. Yu, X. Yang, X. Ma, M. Lin, C. Shao, Y. Zhao, F. Wang, M. Ge, *Catal. Today*, **2019**, *332*, 153-159.
- [21] a) Q. Zhang, J. Hu, P. Ning, X. Liu, H. Wang, G. Wei, T. Zhang, *J. Taiwan Inst. Chem. Eng.* **2019**, *97*, 280-287; b) W. Si, Y. Wang, Y. Peng, X. Li, K. Li, J. Li, *Chem. Commun.* **2015**, *51*, 14977-14980.
- [22] H. C. Genuino, Y. Meng, D. T. Horvath, C.-H. Kuo, M. S. Seraji, A. M. Morey, R. L. Joesten, S. L. Suib, *ChemCatChem*, **2013**, *5*, 2306-2317.
- [23] a) R. Xu, X. Wang, D. Wang, K. Zhou, Y. Li, *J. Catal.* **2006**, *237*, 426-430; b) C. Wang, X. Zou, H. Liu, T. Chen, S. L. Suib, D. Chen, J. Xie, M. Li, F. Sun, *Appl. Surf. Sci.* **2019**, *486*, 420-430.
- [24] a) Y. Wang, W. Deng, Y. Wang, L. Guo, T. Ishihara, *Mol. Catal.* **2018**, *459*, 61-70; b) S. Besselmann, E. Löffler, M. Muhler, *J. Mol. Catal. A.* **2000**, *162*, 401-411; c) H. Einaga, S. Futamura, *J. Catal.* **2006**, *243*, 446-450; d) S. Mo, Q. Zhang, M. Zhang, Q. Zhang, J. Li, M. Fu, J. Wu, P. Chen, D. Ye, *Nanoscale Horiz.* **2019**, *4*, 1425-1433.
- [25] H. Sun, Z. Liu, S. Chen, X. Quan, *Chem. Eng. J.* **2015**, *270*, 58-65.
- [26] a) Q. Zhang, W. Su, P. Ning, X. Liu, H. Wang, J. Hu, *Chem. Eng. Sci.* **2019**, *205*, 230-237.
- [27] a) W. Xu, N. Wang, Y. Chen, J. Chen, X. Xu, L. Yu, L. Chen, J. Wu, M. Fu, A. Zhu, D. Ye, *Catal. Commun.* **2016**, *84*, 61-66; b) J. Du, Z. Qu, C. Dong, L. Song, Y. Qin, N. Huang, *Appl. Surf. Sci.* **2018**, *433*, 1025-1035.

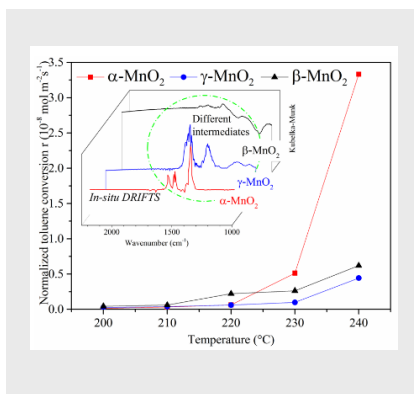
FULL PAPER

Entry for the Table of Contents (Please choose one layout)

Layout 1:

FULL PAPER

α -MnO₂, γ -MnO₂ and β -MnO₂ were synthesized for catalytic oxidation of toluene, and higher r_{norm} was obtained over α -MnO₂. Different intermediates were detected on the surfaces of α -, γ - and β -MnO₂ via in-situ DRIFTS.



Author(s), Corresponding Author(s)*

Page No. – Page No.

Title

Accepted Manuscript